JACS
JOURNAL OF THE AMERICAN CHEMICAL SOCIETY

COMMUNICATION

pubs.acs.org/JACS

An *n*-Channel Two-Dimensional Covalent Organic Framework

Xuesong Ding,[†,¶] Long Chen,[†,¶] Yoshihito Honsho,[‡] Xiao Feng,[†] Oraphan Saengsawang,[§,⊥] Jingdong Guo,[∥] Akinori Saeki,[‡] Shu Seki,[*,‡] Stephan Irle,[§] Shigeru Nagase,[∥] Vudhichai Parasuk,[⊥] and Donglin Jiang[*,†,#]

[†]Department of Materials Molecular Science, Institute for Molecular Science, National Institutes of Natural Sciences, 5-1 Higashiyama, Myodaiji, Okazaki 444-8787, Japan

[‡]Department of Applied Chemistry, Graduate School of Engineering, Osaka University, 2-1 Yamadaoka, Suita, Osaka 565-0871, Japan

[§]Department of Chemistry, Graduate School of Science, Nagoya University, Furo-cho, Chikusa-ku, Nagoya 464-8601, Japan

[⊥]Computational Chemistry Unit Cell, Department of Chemistry, Chulalongkorn University, Phyathai Road, Patumwan, Bangkok 10330, Thailand

[∥]Department of Theoretical and Computational Molecular Science, Institute for Molecular Science, National Institutes of Natural Sciences, 38 Nishigo-naka, Myodaiji, Okazaki 444-8585, Japan

[#]PRESTO, Japan Science and Technology Agency, Chiyoda-ku, Tokyo 102-0075, Japan

Supporting Information

ABSTRACT: Co-condensation of metallophthalocyanine with an electron-deficient benzothiadiazole (BTDA) block leads to the formation of a two-dimensional covalent organic framework (2D-NiPc-BTDA COF) that assumes a belt shape and consists of AA stacking of 2D polymer sheets. Integration of BTDA blocks at the edges of a tetragonal metallophthalocyanine COF causes drastic changes in the carrier-transport mode and a switch from a hole-transporting skeleton to an electron-transporting framework. 2D-NiPc-BTDA COF exhibits broad and enhanced absorbance up to 1000 nm, shows panchromatic photoconductivity, is highly sensitive to near-infrared photons, and has excellent electron mobility as high as 0.6 $cm^2 V^{-1} s^{-1}$.

Covalent organic frameworks (COFs) are a class of crystalline materials with predesignable compositions and porous structures.[1−7] COFs have emerged as a new material for gas adsorption as well as a novel platform for the design of π-electronic skeletons. In this context, two-dimensional COFs offer a unique way to construct π-electronic 2D polymers with eclipsed stacking of aromatic components.[3−7] Such a stacking alignment provides a pathway for charge carrier transport.[7a] Previously, p-type 2D COFs for hole transport have been reported,[3] but electron-transporting 2D COFs are unprecedented. Here we report the synthesis of an n-channel conducting COF and highlight its high-mobility electron-transporting property and prominent photoconductivity.

Our strategy is to employ electron-withdrawing blocks for the construction of n-channel 2D COFs. We placed an electron-deficient building block, benzothiadiazole (BTDA), at the edges of a two-component tetragonal nickel(II) phthalocyanine COF (Chart 1A, 2D-NiPc-BTDA COF). Integration of BTDA units into the 2D COF caused a drastic change in the carrier-transport mode from a hole-transporting to an electron-conducting framework. Owing to the eclipsed stacking arrangement of the 2D polymer sheets (Chart 1B), 2D-NiPc-BTDA COF exhibited excellent electron mobility as high as 0.6 $cm^2 V^{-1} s^{-1}$. This is in sharp contrast to the hole-transporting nature of the nickel(II) phthalocyanine COF that bears phenyl units at the edges of the framework (NiPc COF).[3c]

Chart 1. (A) Schematic Representation of the Synthesis of 2D-NiPc-BTDA COF with Metallophthalocyanine at the Vertices and BTDA at the Edges of the Tetragonal Framework, and (B) Top and Side Views of a Graphical Representation of a 2×2 Tetragonal Grid Showing the Eclipsed Stacking of 2D Polymer Sheets (Pc, sky blue; BTDA, violet; Ni, green; N, blue; S, yellow; O, red; B, orange; and H, white)

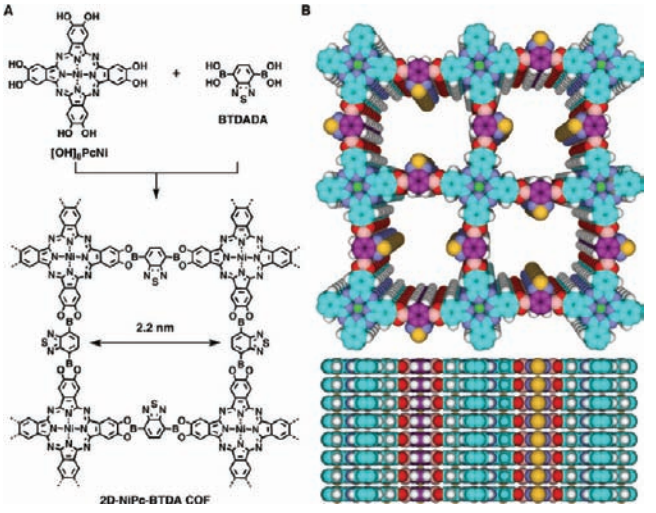

2D-NiPc-BTDA COF was synthesized by condensation of (2,3,9,10,16,17,23,24-octahydroxyphthalocyaninato)nickel(II) ([OH]$_8$PcNi) and 1,4-benzothiadiazole diboronic acid (BTDADA) in a mixture of *o*-dichlorobenzene and dimethylacetamide (1/2 v/v) under solvothermal condition in 85% isolated yield (Supporting Information (SI)). Infrared spectroscopy revealed the formation

Received: June 7, 2011
Published: August 24, 2011

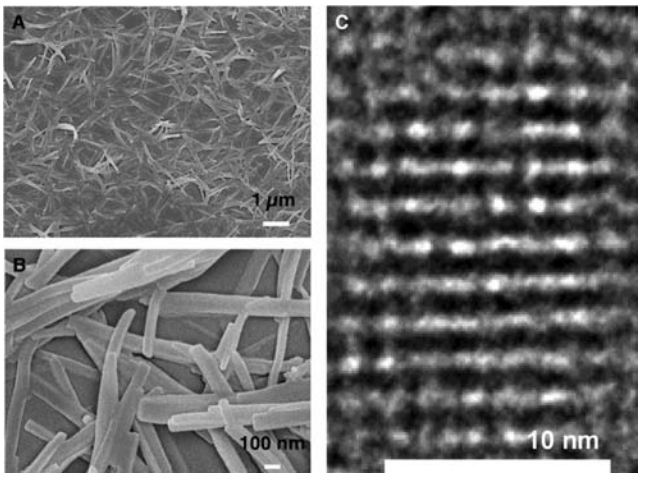

Figure 1. FE-SEM images at (A) low and (B) high magnifications. (C) HR-TEM image.

of ester linkages between NiPc and BTDA in 2D-NiPc-BTDA COF (Figure S1, Table S1). Elemental analyses showed the content of C, H, and N to be 48.6, 2.0, and 16.7%, respectively. Field-emission scanning electron microscopy (FE-SEM, Figures 1A,B) revealed that 2D-NiPc-BTDA COF assumed a belt shape with lengths of several tens of micrometers and widths of ~100 nm. High-resolution transmission electron microscopy (HR-TEM) allowed the direct visualization of tetragonal pores with widths of ~2.0 nm (Figure 1C).

2D-NiPc-BTDA COFs are crystalline belts that show strong peaks in X-ray diffraction (XRD) at 3.80, 7.68, 11.50, and 27.04°, which are assignable to the 100, 200, 300, and 001 facets, respectively (Figure 2A, blue curve). The XRD pattern is similar to that of NiPc COFs.[3c] The tetragonal pores were simulated with hybrid density functional theory at the B3LYP level using a double-ζ basis set (Lanl2dz) effective core potential (Lanl2 ECP) for Ni atoms and the 3-21G(d) basis set for all other atoms using the Gaussian 03 program,[8] and single-point calculations with basis set Lanl2dz for Ni and 6-31G(d) for the other atoms to improve energies, to predict the orientation of the BTDA units on the edges of the pore (SI). The preferred structure reveals that a D_{2h} geometry—i.e., one of the two BTDA units on opposite edges is inward and the other is outward—had the lowest energy, 2.6 kcal mol^{-1}, among the possible orientation patterns (Figure S3). Based on this structure, Pawley refinement (Figure 2A, green curve) of the experimental XRD pattern confirmed the assignment of the observed diffractions and gave a good match to the observed XRD pattern, as evidenced by their negligible difference (Figure 2A, black curve). The crystalline structure was deduced from the XRD pattern using Reflex implemented in Materials Studio version 4.4. Structure simulation using *P*4 space group no. 81 with parameters $\alpha = \beta = \gamma = 90°$, $a = b = 46.49$ Å and $c = 3.40$ Å (Tables S2 and S3) gave an XRD pattern in good agreement with the experimentally observed one (Figure 2A, red curve). The AA stacking unit cell structures are shown in Figure 2B−D. In contrast, a staggered model offset by distances of $a/2$ and $b/2$ (AB stacking, Figure 2E−G) could not reproduce the experimental XRD pattern (Figure 2A, orange curve). These results indicate that the condensation reaction of $[OH]_8$-PcNi and BTDADA leads to the formation of 2D-NiPc-BTDA

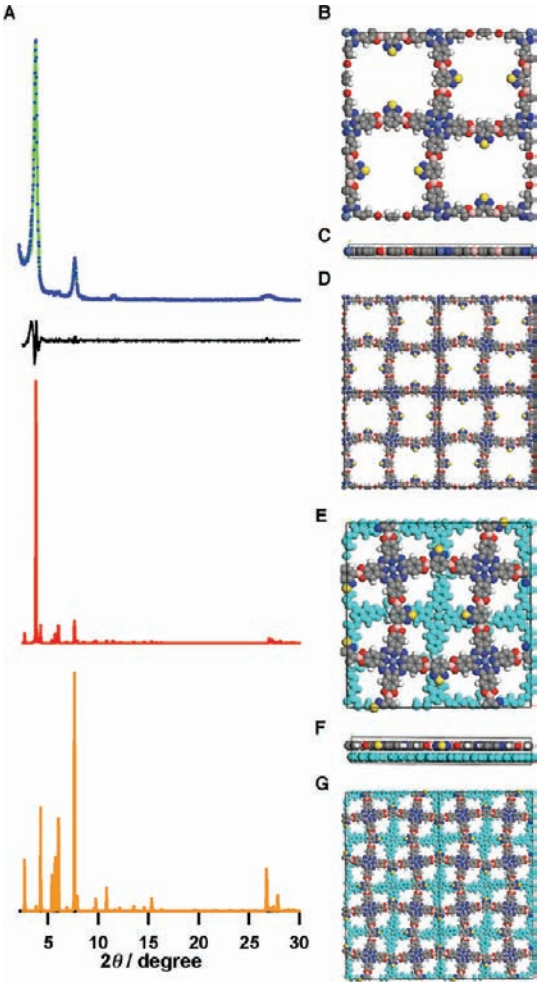

Figure 2. (A) Experimental XRD pattern of 2D-NiPc-BTDA COFs (blue curve), Pawley refined pattern (green curve), their difference (black curve), and simulated XRD patterns using the eclipsed AA stacking (red curve) and staggered AB stacking models (orange curve). Views of the unit cell derived from the AA stacking *P*4 space group along the *z* (B) and *y* axes (C) and a 16-pore structure (D). Views of the 2D staggered structure along the *z* (E) and *y* axes (F) and a staggered stacking 16-pore structure (G).

COFs that assume a belt shape and consist of AA-type stacking of 2D-NiPc-BTDA sheets.

To elucidate the layer structures and stacking energies of 2D-NiPc-BTDA COFs, we applied the density-functional tight-binding method including Lennard-Jones (LJ) dispersion with consideration of periodic boundary conditions. For a 2D monolayer structure, the obtained optimal cell length was $a = b = 46.30$ Å. All atoms form a perfectly planar layer. The optimized stacking distances and the corresponding crystal stacking energies per monolayer and unit cell for both AA and AB forms are summarized in Table S4. The crystal stacking energy for eclipsed AA (312.84 kcal mol^{-1}) is higher than that for stacked AB (178.31 kcal mol^{-1}), indicating a significant energetic preference for AA stacking. AB stacking causes severe loss of π-overlap between the layers, as can be seen by its significantly reduced LJ stacking energy (Table S4). Furthermore, we calculated the AA stacking modes for slightly slipped structures and found that the crystal stacking energies are similar (Table S4). The AA stacking alignment exhibited an optimum stacking distance of 3.4−3.5 Å (Figure S3).

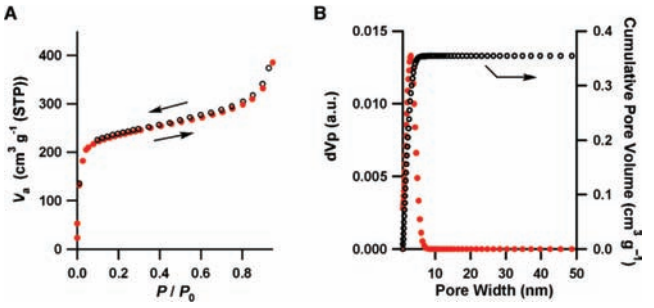

Figure 3. (A) Nitrogen sorption isotherm curves. (B) Pore width and pore width distribution curves.

Accordingly, formation of the AA stacking structure is required by the maximum stacking energy demand for the layered structure.

2D-NiPc-BTDA COF has tetragonal pores with a theoretical width of 2.2 nm. The porous structure was investigated by nitrogen sorption isotherm measurements at 77 K. 2D-NiPc-BTDA COF exhibited reversible isotherm curves (Figure 3A). The Brunauer−Emmett−Teller surface area was evaluated to be 877 $m^2\ g^{-1}$. On the basis of the nonlocal density functional theory model, the pore width was calculated to be 2.2 nm (Figure 3B, red circles), which was identical to the theoretical pore width. The pore width distribution profile (Figure 3B, open circles) revealed that the porosity originated from 2.2-nm-wide pores.

2D-NiPc-BTDA COFs displayed an absorption band at 397 nm (Figure 4A, red curve), which was 15-nm blue-shifted from the B band of the monomeric $[MeO]_8PcNi$ (black curve). The blue-shifted B-band indicated that the phthalocyanine units stacked in the form of H-aggregates, in good agreement with the results of XRD measurements and structure simulations. On the other hand, in the Q-band region, the absorbance was significantly enhanced. The intensity ratio of Q-band to B-band was estimated to be 1.72, which was 1.5-fold as high as that of $[MeO]_8PcNi$. The significantly enhanced absorbance over a broad wavelength range extending up to 1000 nm is interesting for the exploration of photofunction.

The AA stacking arrangement of 2D phthalocyanine sheets provides a pathway for carrier transport. We investigated intrinsic carrier mobility using a flash photolysis time-resolved microwave conductivity (FP-TRMC) method. To discern the charge carrier, the transient conductivity was investigated under different atmospheres of O_2, SF_6 (electron quenchers), and Ar. Excitation with 355-nm pulsed laser at a photon density at 1.6×10^{15} photon cm^{-2} under Ar gave a $\Phi\Sigma\mu$ (Φ is the photocarrier generation yield and $\Sigma\mu$ is the sum of the mobilities of charge carriers) value of $5.8 \times 10^{-4}\ cm^2\ V^{-1}\ s^{-1}$ (Figure 4B, red curve). The double-exponential decay curve kinetics (Figure S4, Table S5) is related to the kinetic trace of conductivity transients of electrons (first decay) and holes (second decay). The first decay was considerably accelerated when measured under SF_6 (blue curve) or upon annealing under SF_6 (orange and green curves) or O_2 (black curve), supporting that the fast decay component was due to the mobile electrons. In contrast, the second decay component was almost independent for the SF_6 and O_2 annealed samples, and the pre-exponential factor of the second decay component gave a $\Phi\Sigma\mu$ the value of only $2.9 \times 10^{-5}\ cm^2\ V^{-1} s^{-1}$ for the holes.

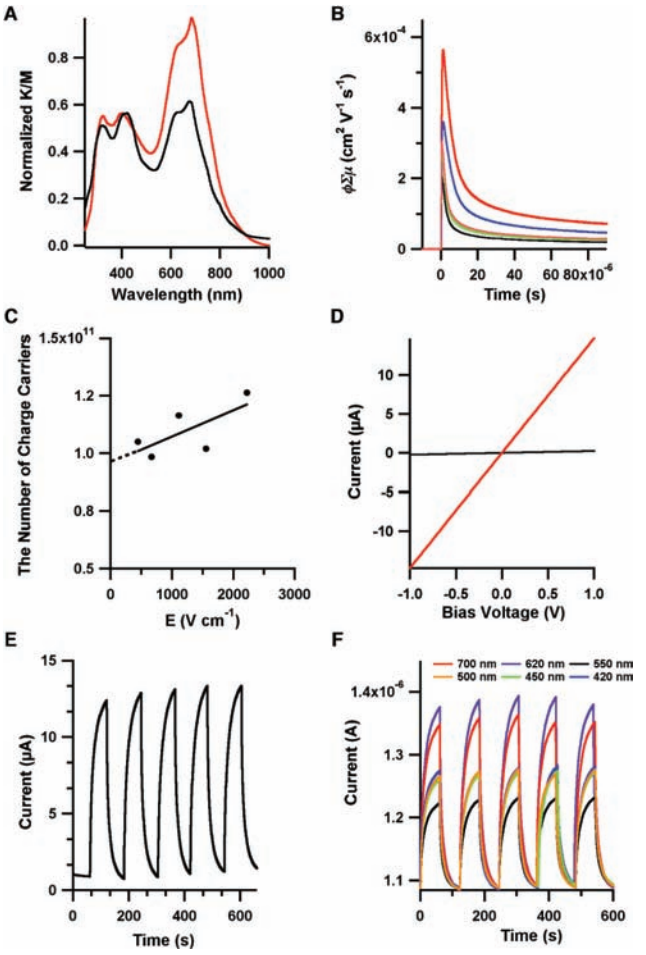

Figure 4. (A) Electronic absorption spectra of 2D-NiPc-BTDA COFs (red curve) and $[MeO]_8PcNi$ (black curve). (B) Transient conductivities irradiated with a 355-nm pulsed laser at the photon density of 1.6×10^{15} under Ar (red curve), SF_6 (blue curve), and after annealing under SF_6 for 1 h (orange curve) and 24 h (green curve) or under O_2 for 24 h (black curve). (C) Number of charge carriers measured by the time-of-flight transient current integration at different bias voltages, irradiated with a 355-nm pulsed laser of 5.0×10^{14} photons cm^{-2}. (D) $I-V$ curves of 2D-NiPc-BTDA COFs in the dark (black curve) and upon irradiation (red curve) with visible light. (E) On−off switching of photocurrent of 2D-NiPc-BTDA COFs at the bias voltage of 1.0 V, by switching the light on and off. (F) Wavelength-dependent on−off switching of photocurrent at the bias voltage of 1.0 V.

To determine the yield of photocarrier generation, the time-of-flight transient conductivity was integrated at different bias voltages at a photon density of 5.0×10^{14} photons cm^{-2} (Figure 4C). The number of charge carriers estimated by extrapolation of the bias at 0 V was 9.6×10^{10}, leading to $\Phi = 9.2 \times 10^{-4}$. Thus, 2D-NiPc-BTDA COFs are electron-transporting frameworks with outstanding mobility as high as $0.6\ cm^2\ V^{-1}\ s^{-1}$.

The AA stacking arrangement of 2D polymer sheets endows 2D-NiPc-BTDA COFs with efficient absorbance over a wide range of wavelengths from the visible to the near-infrared region up to 1000 nm and excellent electron-transporting property. Along this line, we investigated the photoconductivity of 2D-NiPc-BTDA COFs. Upon irradiation with visible light (>400 nm), 2D-NiPc-BTDA COFs exhibited an enhanced photocurrent from 250 nA to 15 μA (Figure 4D). The photocurrent can be switched

on−off many times without deterioration (Figure 4E). To probe the wavelength-dependent response, we utilized band-path filters for selective excitation of 2D-NiPc-BTDA COFs at different wavelengths. Interestingly, 2D-NiPc-BTDA COFs were panchromatic responsive and exhibited extreme sensitivity to near-infrared photons (Figure 4F). Photoconductive COFs with vertically aligned π columns are interesting for the development of organic electronics. 2D-NiPc-BTDA-COF is unique because it is an n-channel semiconductor combining broad absorbance up to 1000 nm, panchromatic photoconductivity, and high IR sensitivity. Such an n-type semiconductor is unprecedented.

In summary, we have developed a strategy for the synthesis of the first example of n-type semiconducting 2D COFs using electron-withdrawing blocks. 2D-NiPc-BTDA COFs adopt AA-type stacking arrangement and exhibit enhanced absorbance over a wide range of wavelengths up to 1000 nm; they exhibit panchromatic photoconductivity and are highly sensitive to near-infrared lights. Owing to the AA-type stacking, 2D-NiPc-BTDA COFs provide pathways for carrier transport. As a result, the n-channel 2D-NiPc-BTDA COFs transport electrons with high carrier mobility. These characteristics clearly originate from the structural features of the 2D COFs and are hard to achieve with other n-type semiconductors; thus, this constitutes a new aspect in the design of π-electronic fucntions of COFs.

■ ASSOCIATED CONTENT

Supporting Information. Complete ref 8, detailed experimental procedures, FT IR spectra, and simulations. This material is available free of charge via the Internet at http://pubs.acs.org.

■ AUTHOR INFORMATION

Corresponding Author

seki@chem.eng.u-osaka.ac.jp; jiang@ims.ac.jp

Author Contributions

¶These authors contributed equally.

■ ACKNOWLEDGMENT

We are grateful for the financial support of PRESTO, JST. O.S. thanks the National Research University Project of CHE and the Ratchadaphiseksomphot Endowment Fund (AM1078I) for financial support and a postdoctoral fellowship.

■ REFERENCES

(1) (a) Côté, A. P.; Benin, A. I.; Ockwig, N. W.; O'Keeffe, M.; Matzger, A. J.; Yaghi, O. M. *Science* **2005**, *310*, 1166. (b) Côté, A. P.; El-Kaderi, H. M.; Furukawa, H.; Hunt, J. R.; Yaghi, O. M. *J. Am. Chem. Soc.* **2007**, *129*, 12914. (c) El-Kaderi, H. M.; Hunt, J. R.; Mendoza-Cortés, J. L.; Côté, A. P.; Taylor, R. E.; O'Keeffe, M.; Yaghi, O. M. *Science* **2007**, *316*, 268. (d) Han, S. S.; Furukawa, H.; Yaghi, O. M.; Goddard, W. A., III *J. Am. Chem. Soc.* **2008**, *130*, 11580. (e) Hunt, J. R.; Doonan, C. J.; LeVangie, J .D.; Côté, A. P.; Yaghi, O. M. *J. Am. Chem. Soc.* **2008**, *130*, 11872. (f) Uribe-Romo, F. J.; Hunt, J. R.; Furukawa, H.; Klock, C.; O'Keeffe, M.; Yaghi, O. M. *J. Am. Chem. Soc.* **2009**, *131*, 4570. (g) Furukawa, H.; Yaghi, O. M. *J. Am. Chem. Soc.* **2009**, *131*, 8875. (h) Doonan, C. J.; Tranchemontagne, D. J.; Glover, T. G.; Hunt, J. H.; Yaghi, O. M. *Nature Chem.* **2010**, *2*, 235.

(2) (a) Tilford, R. W.; Gemmill, W. R.; zur Loye, H. C.; Lavigne, J. J. *Chem. Mater.* **2006**, *18*, 5296. (b) Tilford, R. W.; Mugavero, S. J., III; Pellechia, P. J.; Lavigne, J. J. *Adv. Mater.* **2008**, *20*, 2741.

(3) (a) Wan, S.; Guo, J.; Kim, J.; Ihee, H.; Jiang, D. *Angew. Chem., Int. Ed.* **2008**, *47*, 8826. (b) Wan, S.; Guo, J.; Kim, J.; Ihee, H.; Jiang, D. *Angew. Chem., Int. Ed.* **2009**, *48*, 5439. (c) Ding, X.; Guo, J.; Feng, X.; Honsho, Y.; Guo, J.; Seki, S.; Maitarad, P.; Saeki, A.; Nagase, S.; Jiang, D. *Angew. Chem., Int. Ed.* **2011**, *50*, 1289. (d) Feng, X.; Chen, L.; Dong, Y.; Jiang, D. *Chem. Commun.* **2011**, *47*, 1979.

(4) (a) Kuhn, P.; Antonietti, M.; Thomas, A. *Angew. Chem., Int. Ed.* **2008**, *47*, 3450. (b) Wang, X.; Maeda, K.; Thomas, A.; Takanabe, K.; Xin, G.; Carlsson, J. M.; Domen, K.; Antonietti, M. *Nat. Mater.* **2008**, *8*, 76. (c) Bojdys, M. J.; Jeromenok, J.; Thomas, A.; Antonietti, M. *Adv. Mater.* **2010**, *22*, 2202.

(5) (a) Campbell, N. L.; Clowes, R.; Ritchie, L. K.; Cooper, A. I. *Chem. Mater.* **2009**, *21*, 204. (b) Hasell, T.; Wu, X.; Jones, J. T. A.; Bacsa, J.; Steiner, A.; Mitra, T.; Trewin, A.; Adams, D. J.; Cooper, A. I. *Nature Chem.* **2010**, *2*, 750.

(6) (a) Spitler, E. L.; Dichtel, W. R. *Nature Chem.* **2010**, *2*, 672. (b) Colson, J. W.; Woll, A. R.; Mukherjee, A.; Levendorf, M. P.; Spitler, E. L.; Shields, V. B.; Spencer, M. G.; Park, J.; Dichtel, W. R. *Science* **2011**, *332*, 228.

(7) (a) Patwardhan, S.; Kocherzhenko, A. A.; Grozema, F. C.; Siebbeles, L. D. A. *J. Phys. Chem. C* **2011**, *115*, 11768. (b) Lukose, B.; Kuc, A.; Heine, T. *Chem.—Eur. J.* **2011**, *17*, 2388. (c) Farha, O. K.; Spokoyny, A. M.; Hauser, B. G.; Bae, Y.-S.; Brown, S. E.; Snurr, R. Q.; Mirkin, C. A.; Hupp, J. T. *Chem. Mater.* **2009**, *21*, 3033. (d) Dogru, M.; Sonnauer, A.; Gavryushin, A.; Knochel, P.; Bein, T. *Chem. Commun.* **2011**, *47*, 1707.

(8) Frisch, M. J.; et al. *Gaussian 03*, revision E.01; Gaussian, Inc.: Wallingford, CT, 2004.